Geophysical Journal International

Geophys. J. Int. (2017) **208,** 508–520
Advance Access publication 2016 November 17
GJI Seismology

doi: 10.1093/gji/ggw418

3-D seismic tomographic modelling of the crustal structure of northwestern Svalbard based on deep seismic soundings

Wojciech Czuba

Institute of Geophysics, Polish Academy of Sciences, ks. Janusza 64, 01–452 *Warsaw, Poland. E-mail: wojt@igf.edu.pl*

Accepted 2016 November 4. Received 2016 November 2; in original form 2015 August 24

SUMMARY

Wide angle refraction and reflection measurements were carried out in the passive continental margin zone of the northwestern Svalbard during several expeditions in 1978–1999. Data from a set of 2-D archival and modern seismic profiles recorded in-line and off-line, and from an additional permanent seismic station, were altogether used for seismic modelling of the crustal structure of the study area. Seismic arrivals (airgun and chemical explosive sources) were recorded by land (onshore) seismic stations, ocean bottom seismometers (OBS), and ocean bottom hydrophone stations (OBH). Good quality refracted and reflected *P* waves have provided an excellent data base for a seismic modelling. Chemical explosive sources were recorded even up to 300 km distances. The 3-D tomographic inversion method was applied. The results are comparable to the earlier 2-D modelling. Additional off-line information allowed to develop a 3-D image of the crustal structure. The continental crust thins to the west and north. A minimum depth of about 6 km to the Moho interface was determined east of the Molloy Deep and in the Knipovich Ridge. The Moho discontinuity deepens down to about 30 km below the continental crust of Spitsbergen.

Key words: Controlled source seismology; Seismic tomography; Crustal structure; Arctic region; Atlantic Ocean.

1 INTRODUCTION

Svalbard Archipelago is located in the northwestern corner of the Barents Sea continental platform. It is bordered by passive continental margins to the west and north (Fig. 1a). This Arctic region is the crucial area to understand the tectonic evolution of the North Atlantic and Arctic Oceans. As one of the youngest region of the Oceans it gives a good chance to investigate processes leading to their opening. Transform movement, rifting and subsequent seafloor spreading in the North Atlantic Ocean, and the development of the passive sheared continental margin of the Barents Sea continental platform are the processes which drove the tectonic evolution of the region. The evolution of this region is strongly connected to the history of rifting and subsequent seafloor spreading in the North Atlantic Ocean (Jackson *et al.* 1990; Lyberis & Manby 1993a; Lyberis & Manby 1993b; Ohta 1994).

The Svalbard passive continental margin and its continent–ocean transition zone have been studied by geophysical methods over the years including multichannel seismic reflection, sonobuoy seismic refraction, gravity and magnetics. The continent–ocean boundary (COB) in the region between Svalbard Archipelago in the north and Scandinavia in the south has been relatively well investigated by using multichannel reflection seismics—for review see for example, Gabrielsen *et al.* (1990) and Faleide *et al.* (2008), and by gravity modelling (e.g. Breivik *et al.* 1999). Nevertheless, all these investigations provided only limited information about the crystalline basement and the deep crustal structure of this area.

Deep seismic sounding using the refraction technique generally provides information about the crystalline basement and crust-mantle transition (e.g. Davydova *et al.* 1985; Faleide *et al.* 1991; Mjelde *et al.* 2002; Ljones *et al.* 2004). It provides constraints on the lithospheric structure, tectonics as well as some insights on the hydrocarbon potential.

This paper is focused on the 3-D seismic modelling and crustal structure of the northeastern Spitsbergen area, within the Svalbard Archipelago, based on wide-angle seismic refraction and reflection studies (WARR) acquired in the continent–ocean transition zone of the northwestern Svalbard margin during the international expeditions in 1978–1999 (Fig. 1). The purpose of this study is to constrain a 3-D image of the crustal structure by a real 3-D seismic modelling scheme, not only based on interpolation and extrapolation of 2-D profiles.

After the seismic reconnaissance in 1976 (Guterch *et al.* 1978), geophysical experiments were performed in 1978 (Sellevoll *et al.* 1991), 1985 (Czuba *et al.* 1999) and 1999 (Jokat *et al.* 2000) by Polish and international expeditions. The seismic energy generated by chemical charges (tri-nitro toluene – TNT) and airgun shots was recorded in-line and off-line by vertical component seismic land receivers, ocean bottom hydrophones (OBH) and three-component ocean bottom seismometers (OBS). The data from 1999 was additionally recorded by the Isfjorden NORSAR seismic station

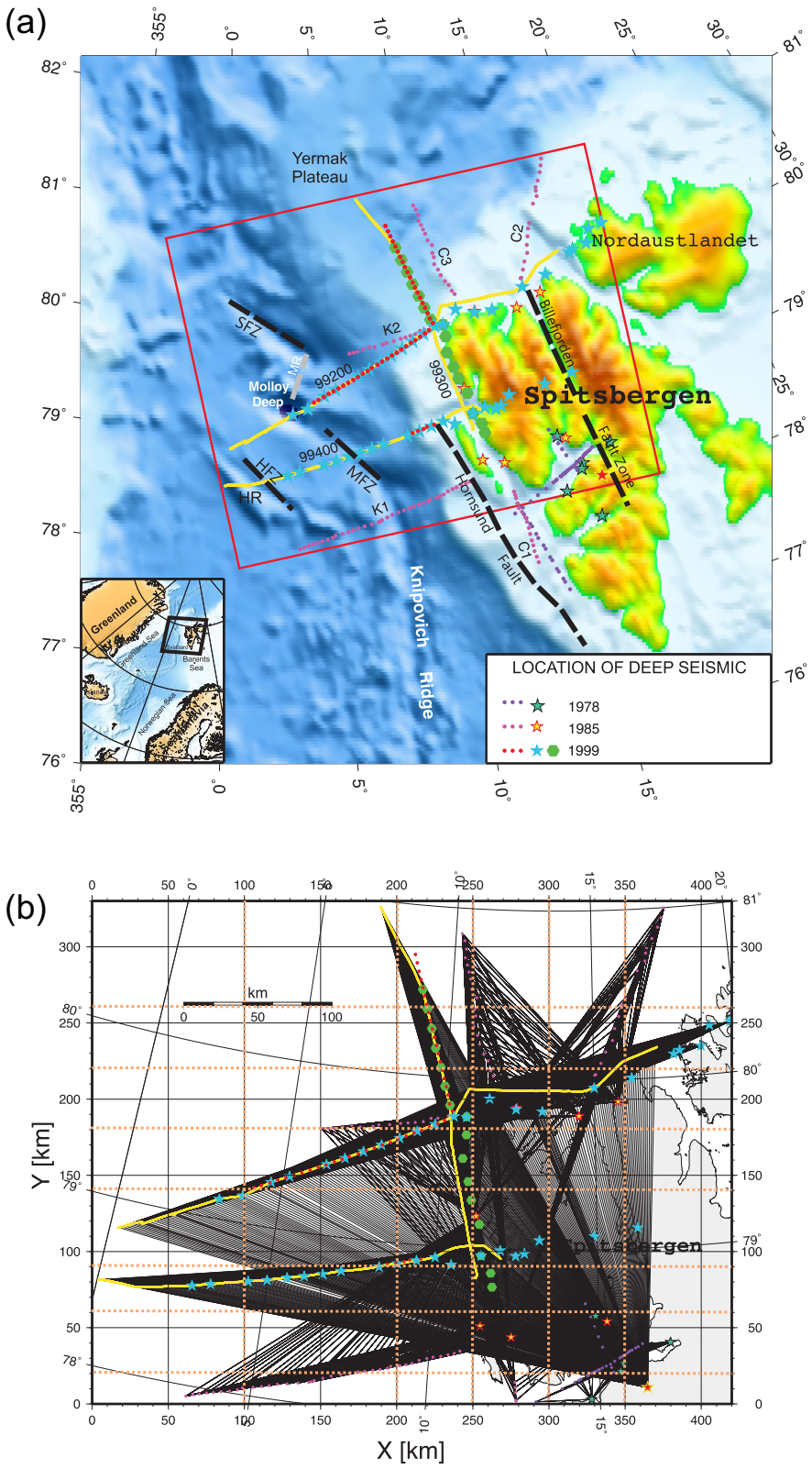

Figure 1. (a) Location map of the seismic study area in the northwestern Svalbard region. Stars and hexagons are receivers, yellow lines and coloured dots are airgun and chemical shots along the seismic profiles. The red rectangular frame marks the 3-D modelling area. HFZ, Hovgård Fracture Zone; HR, Hovgård Ridge; MFZ, Molloy Transform Fault Zone; MR, Molloy Ridge; SFZ, Spitsbergen Transform Fault Zone. (b) Map of the 3-D modelling area in geographical and Cartesian (km) coordinates. Thin black lines – 10 per cent of airgun and all the TNT seismic ray paths connecting the sources and receivers. Light brown lines mark location of model slices presented in Fig. 4. Other descriptions as in (a).

(SPITS). Good seismic records from airgun shots were obtained up to 200 km distances at onshore stations and up to 50 km at OBSs. TNT shooting was recorded even up to 300 km distances along the profiles. The field work, experiment set-up and 2-D interpretation results are described in details in previous publications (i.e. Sellevoll *et al.* 1991; Czuba *et al.* 1999, 2005; Jokat *et al.* 2000; Ritzmann & Jokat 2003).

2 GEOLOGY AND TECTONICS OF THE INVESTIGATION AREA

The geological history of Svalbard Archipelago reflects the relative activity of the Eurasian and the North American plates (Eldholm *et al.* 1987), and can be divided in several prominent tectonic stages (e.g. Birkenmajer 1993; Ohta 1994; Harland 1997; Dallmann 1999). A graben system was developed in the late Devonian, during the Svalbardian Phase, which is considered to be a late phase of the Caledonian orogeny (Dallmann 1999). There were no further large-scale tectonic events in the North Atlantic region until the Carboniferous times (Torsvik *et al.* 1985). The Mesozoic stratigraphy consists mainly of shelf sediments (Steel & Worsley 1984). The transform faulting between Greenland and the Barents Sea in the Early Mesozoic was not recorded in Svalbard (Birkelund & Håkansson 1983; Håkansson *et al.* 1991). The first records of continental break-up between Greenland and Europe in Svalbard come from the late Jurassic. Basaltic lavas were extruded during the Early Cretaceous in eastern Svalbard (Burov *et al.* 1977). Cenozoic tectonic processes in the Svalbard area are related to the structural history of the western Barents Sea margin. The relative motion between Svalbard and Greenland occurred along the Hornsund Fault Zone, traced from just south of Bjørnøya at *ca*. 75°N to about 79°N (Sundvor & Eldholm 1979, 1980). This regional fault zone has acted as an incipient plate boundary between the opening Arctic Ocean and the Barents Sea shelf. The initial opening of the southern Greenland Sea apparently began in the early Eocene (Faleide *et al.* 1988), but no significant separation between Svalbard and Greenland occurred until about 36 Ma. The next phase of North Atlantic evolution was marked by a change in the spreading direction from NNW–SSE to NW–SE. This begun in the Early Oligocene when spreading in the Labrador Sea stopped (Talwani & Eldholm 1977; Mosar *et al.* 2002). The beginning of the phase unlocked the northward development of the Mid-Atlantic Ridge. The spreading axis developed into the Spitsbergen Shear Zone creating the asymmetric, ultraslow and obliquely spreading Knipovich Ridge. Around 23 Ma, spreading started along the Molloy Ridge and around 10 Ma continental break-up occurred along the Fram Strait. This established a connection between the Arctic and the Northern Atlantic ridges (Crane *et al.* 1991; Lundin & Doré 2002).

The Yermak Plateau is another major tectonic structure, located north of Spitsbergen. It was considered as a volcanic body probably related to the early spreading along the Gakkel Ridge (Feden *et al.* 1979). However, recent results suggest that, at least, the southwestern part of the Yermak Plateau is a fragment of the Svalbard continental crust, with no indications of extensive volcanic activity in the middle and lower crust (Ritzmann & Jokat 2003).

3 SEISMIC PROCESSING AND MODELLING

Generally, good quality records allowed a detailed investigation of the seismic wave field and crustal structure in the study area (Fig. 1). Full specification of the wave field and seismic data processing has been presented in previous publications (i.e. Czuba *et al.* 1999, 2004, 2005; Ritzmann & Jokat 2003). Additional off-line seismic records were incorporated and new seismic arrivals were picked. These records were not taken into account during previous 2-D interpretations. Only vertical component records and main, clearly visible, seismic arrivals were used in this study. Theoretical ray paths between sources and receivers are schematically presented in Fig. 1(b) in the frame of the 3-D model area of 420 km × 330 km. The geometry setup of the seismic measurements in the study area was not planned as 3-D acquisition, however, a compilation of the records from several projects gives a 3-D coverage of the study area. This feature is clearly visible in Fig. 1(b). The ray coverage is not as dense as it would be in a truly 3-D planned experiment; nevertheless, it allows to use a 3-D seismic modelling approach. The model space with no ray coverage between the constrained areas is automatically interpolated during inversion by the JIVE3D software. The external areas are extrapolated by the JIVE3D modelling software.

Examples of record sections are presented in Figs 2 and 3. The most spectacular feature is shown in Fig. 2(a). It is a record section from the OBS deployed in the Molloy Deep at a depth of about 5 km. The Pg waves are almost absent, but Pn and PmP start just at the station. The phases are well identified during 2-D modelling (Czuba *et al.* 2005). Because of the Moho interface shape, Pn phases were recorded east of the OBS and PmP phases were recorded west of the OBS. Thus, the OBS is located very close to the mantle. Fig. 2(b) shows an example of the original record section from 1985. Every TNT shot was recorded by 5-channel vertical-component land station (the station has recorded signals independently from 5 vertical geophones located in-line every 100–200 m at the station). There are Pg and Pn energy clearly visible up to the end of the profile K1. The comparison of TNT and airgun shots recorded along the same part of the profile 99 200 is presented in Fig. 2(c). Clear first arrivals are present up to 300 km distance in the TNT record section but they are not as sharp as in the airgun record section (labelled as Pn and P1).

Because of the geometry set-up, density of the available data, and software requirements, the area of the 3-D seismic tomographic modelling is chosen to be in a rectangle measuring 420 km × 330 km (Fig. 1). Off-line records provide supplemental data for improving the ray coverage (Figs 1b and 3). Other existing DSS profiles in the Svalbard region (e.g. Czuba 2013) are located outside the study area.

A method based on first arrivals only (e.g. Hole 1992) gives limited information. It is necessary therefore to use other arrivals of reflected and later refracted waves to supplement the model. Therefore the 3-D tomographic software package JIVE3D (Hobro 1999; Hobro *et al.* 2003) was chosen. It uses a layer-interface parametrization (a model is described as a stack of layers separated by interfaces). Input data comprise first and later refracted and reflected arrivals. A model is parametrized using regular grids of velocity and depth nodes for individual layers. Ray tracing and ray perturbation theory methods are used for traveltime calculations. The iterative regularized least-squares method is used as the inversion algorithm.

The modelling area 420 km × 330 km × 60 km (length × width × thickness) was set. The uppermost layer is a fixed water layer. The bathymetry and topography is based on the International Bathymetric Chart of the Arctic Ocean (IBCAO) database (Jakobsson *et al.* 2000). A procedure of using the JIVE3D software package allows every layer and interface to be modelled separately (or jointly a layer with its interface). It is possible to model upper parts of the crust

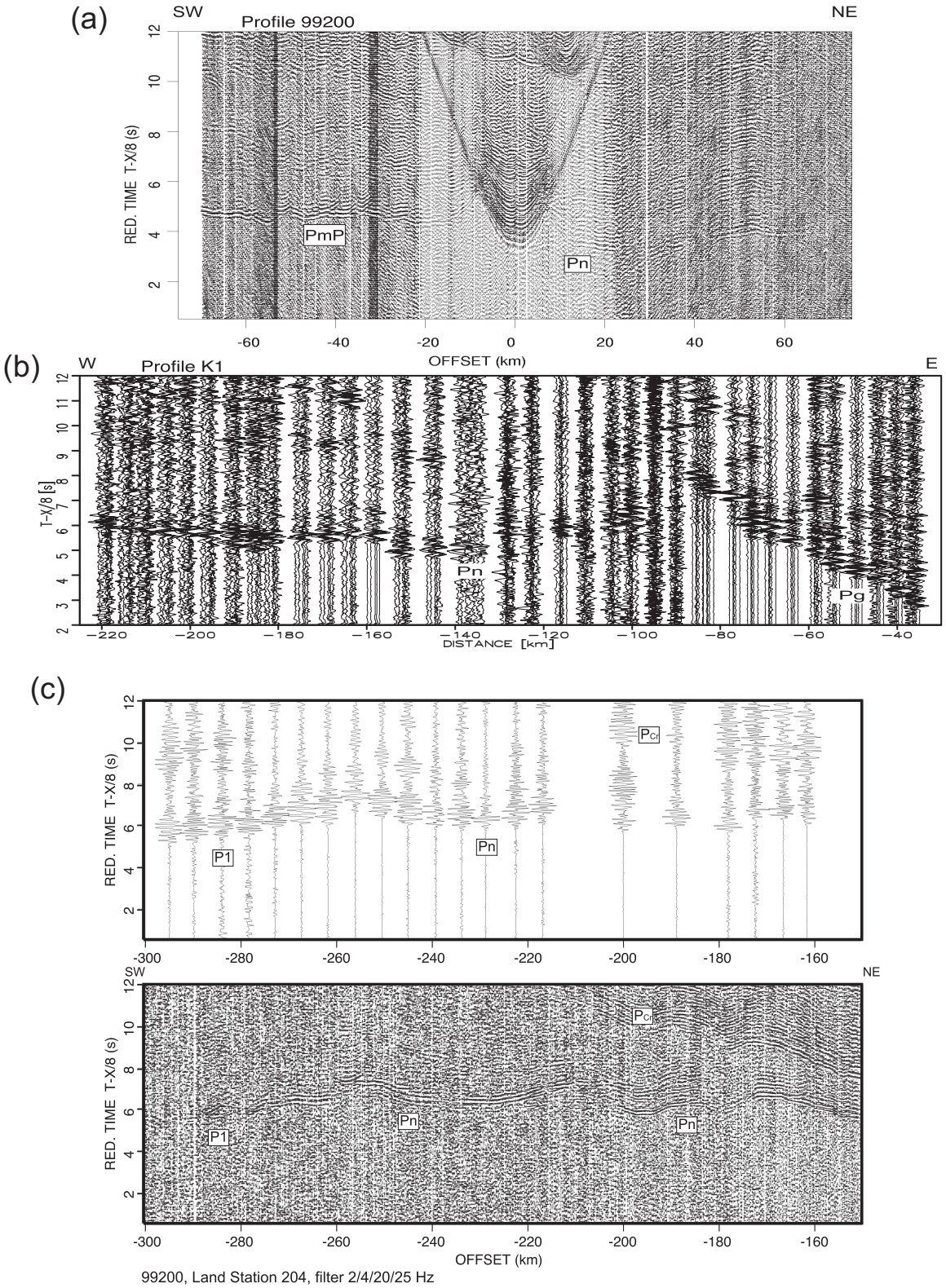

Figure 2. Examples of amplitude-normalized seismic record sections, vertical component, reduction velocity 8 km s^{-1}. (a) Profile 99 200 from 1999, airgun energy recorded by the OBS located in the Molloy Deep. (b) Profile K1 from 1985, TNT shots recorded by 5-channel station located at the western coast of Spitsbergen. (c) Comparison of amplitude-normalized seismic record sections, profile 99 200, land station, top – TNT record section (WT plot), bottom – airgun record section (VA plot). Pg, first arrivals of crustal *P* waves; Pcr, later crustal refracted *P* waves; Pn, refracted *P* waves beneath the Moho; PmP, Moho *P*-wave reflections; P1, lower lithospheric reflections.

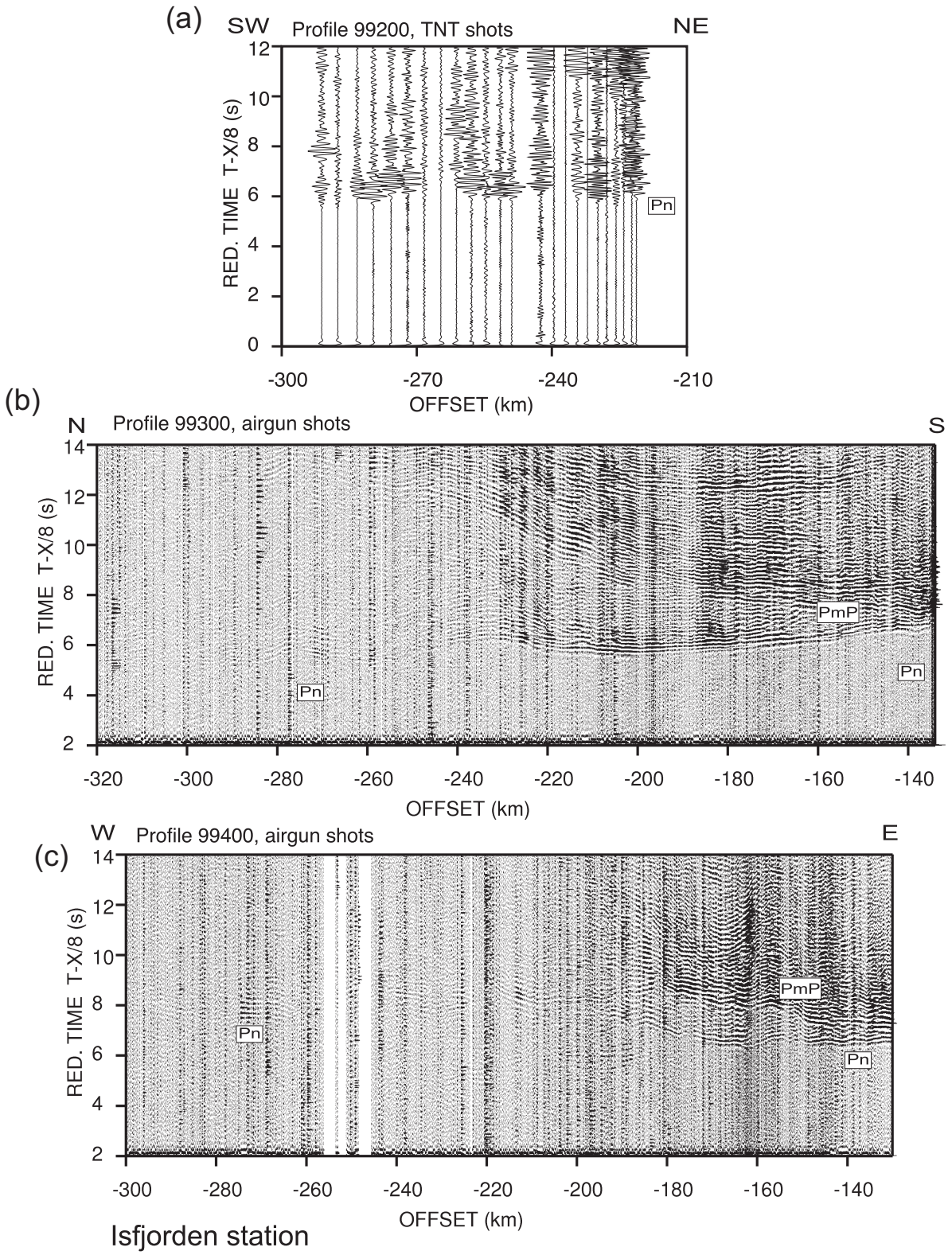

Figure 3. Examples of amplitude-normalized off-line seismic record sections, vertical component, reduction velocity 8 km s^{-1} recorded in Isfjorden NORSAR seismic station (SPITS). (a) Profile 99 200 from 1999, TNT shots. (b) Profile 99 300 from 1999, airgun shots. (c) Profile 99 400 from 1999, airgun shots. Pn, refracted *P* waves beneath the Moho; PmP, Moho *P*-wave reflections.

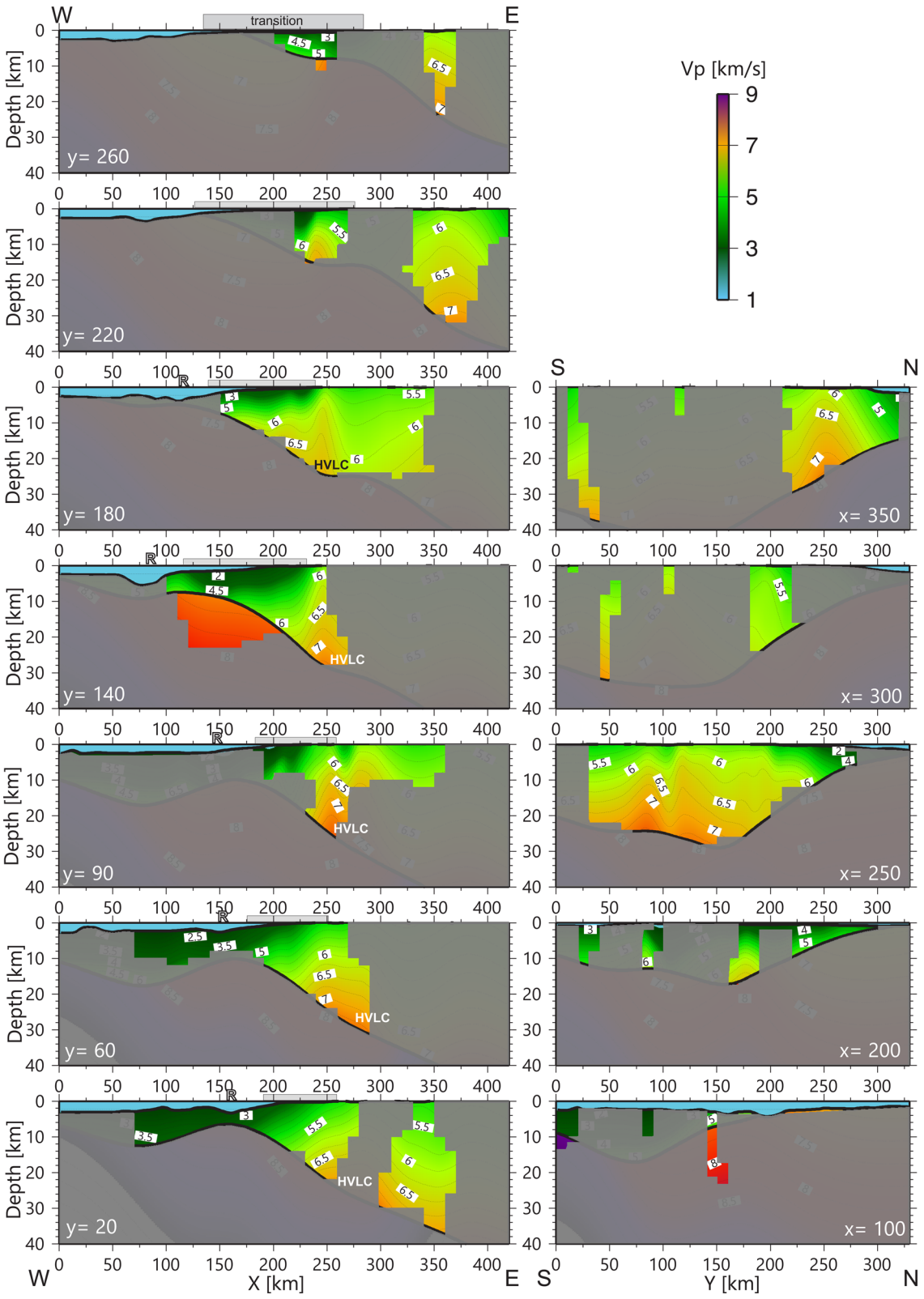

Figure 4. Illustration of the final 3-D model. Examples of vertical sections parallel to the *X*-axis (left-hand column) and parallel to the *Y*-axis (right-hand column). Colours represent the *P*-wave velocity distribution, black thin lines – velocity isolines, black thick lines – sea bottom and Moho boundary, numbers inside white boxes – *P*-wave velocities in km s^{-1}. Grey mask marks poorly constrained parts of the model. Grey bar marks location of the continent-ocean transition zone. Letter R above some slices marks location of the mid-oceanic ridge. HVLC marks high velocity lower crust.

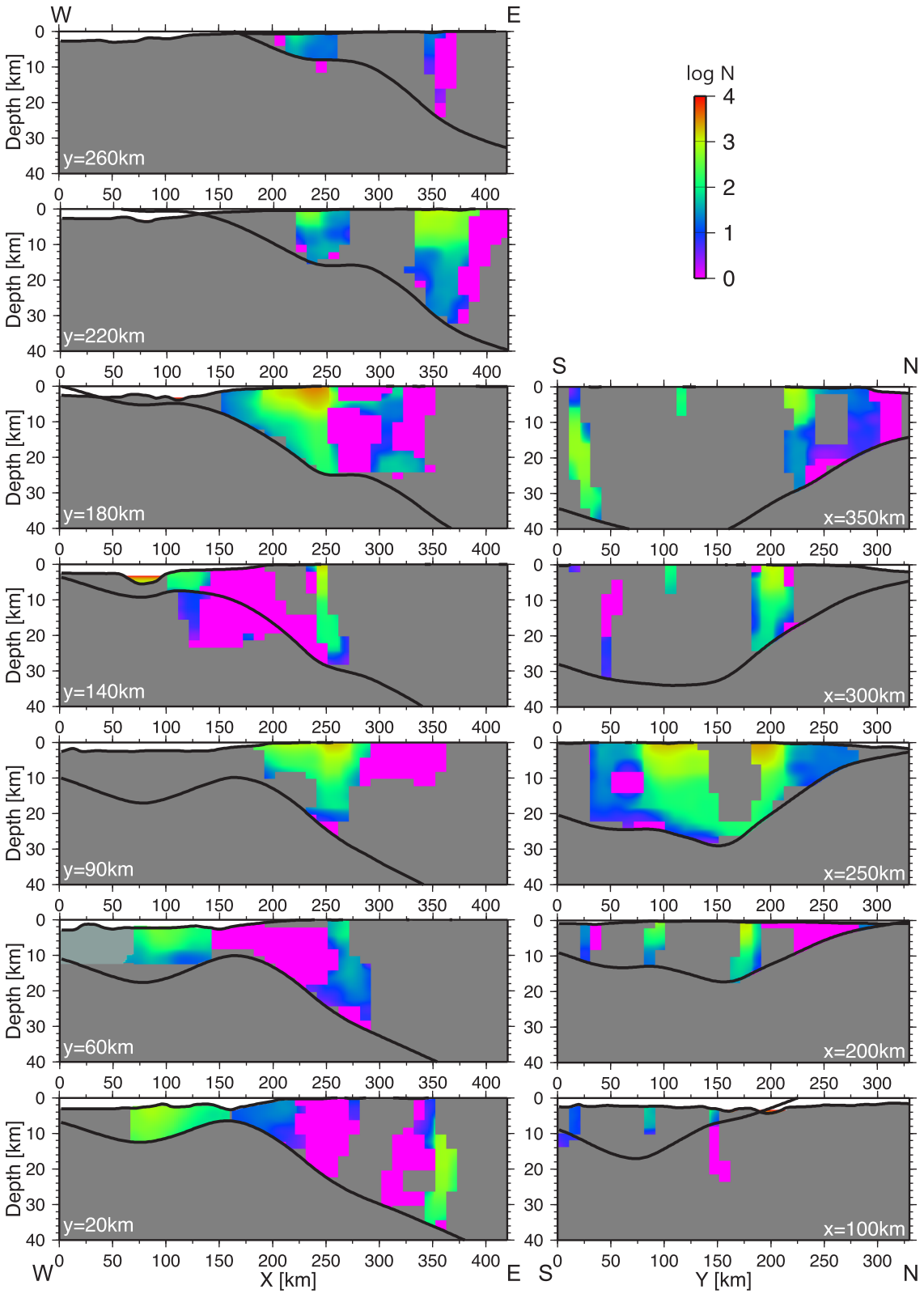

Figure 5. Examples of ray density (in logarithmic scale): vertical sections parallel to the *X*-axis (left-hand column) and parallel to the *Y*-axis (right-hand column) for the final 3-D model. Colours represent number of rays crossing a cell, black lines – sea bottom and Moho boundary.

first, and then separately the underlying deeper layers, based on fixed upper parts. This approach minimizes the number of inversion parameters required to stabilize the whole inversion procedure. The inversion path consists of several steps with different regularization strength that gradually decrease the smoothness of the model. There are a number of iteration loops in every step. The output model from the upper layer modelling is used for the next step of the inversion as an input model. The modelling is stopped when χ^2 is minimalized

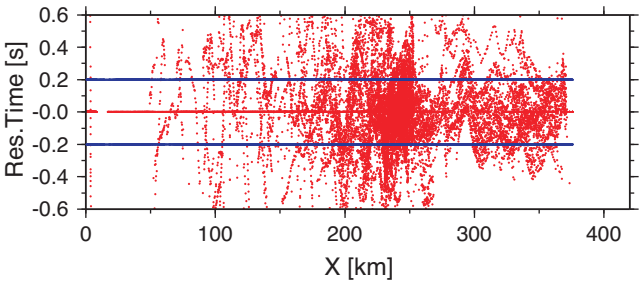

Figure 6. Time residuals. Blue dots – ±0.2 s error limit, red dots – residuals. 62 per cent of picks fits the limit.

and ceased to decrease. The initial 1-D model was defined based on the 2-D model from Czuba *et al.* (2005) and additional inversion tests. Picking errors in arrival times determined by visual estimation of time picking accuracy are of 0.2 s for the first arrivals of refracted waves and waves from sediments (Pg, Pn and Psed), and 0.25 s for Moho reflected waves and later crustal refracted waves (PmP and Pcr).

Taking into account the lowest data density from the oldest measurements (shot points every 5 km), layers and grids are defined as follows:

- Fixed water layer
- Topography and bathymetry: nodes spaced every 2 km
- Crustal layer: velocity nodes spaced every 10 km horizontally and 2 km vertically
- Moho boundary: nodes spaced every 10 km
- Upper mantle: velocity nodes spaced every 10 km horizontally and every 2 km vertically

The regularization strength decreases during calculations according to Hobro (1999). Based on test modelling, parameters for best and relatively fast convergence of the algorithm were chosen. The modelling sequence was performed in two steps. First, the *P*-wave velocity field in the crustal layer (the first layer of the model) using Psed, Pg and Pcr arrivals (first arrivals from refractions in sediments and the crust, and later refractions in the crust, respectively) was calculated. The velocity field was determined also in the lower crust in this step because Pcr waves penetrate deeper layers than Pg waves. The regularization strengths decreased from –3.0 to –4.5 every 0.5 with 2 iterations each, and further the regularization strengths decreased from –5 to –9 every 1.0 with 4 iterations each. χ^2 decreased from 88.5 to 5.1 with hit rate 94 per cent.

Then, the output model was used to calculate the topography of the Moho boundary as well as the *P*-wave velocity field in the upper mantle based on PmP and Pn arrivals. The Moho boundary smoothing factor one level less than general software value was used to allow easier calculation of the Moho slope in the continent–ocean transition zone. It means that the algorithm enables a slightly greater variability of the Moho relative to the other modelling elements. The regularization strengths decreased from –3.5 to –4.5 every 0.5 with 2 iterations each, and further the regularization strengths decreased from –5 to –6 every 1.0 with 4 iterations each. χ^2 decreased from 276.7 to 12.1 with hit rate 67 per cent. The upper mantle velocity field and Moho depth are determined worse than the crust, probably because of poor rays density and many deep ray paths running through the unresolved regions - with no data from the upper part of the model because of not fully 3-D set-up.

In total, 23 075 traveltimes were used. The overall χ^2 value for the final model (Figs 4 and 5) was 6.5 with the hit rate of 81 per cent. Most of the residual times (Fig. 6) are located within the limits of ±0.2 s (38 per cent within the limits ±0.1 s, 62 per cent within the limits ±0.2 s and 84 per cent within the limits ±0.4 s). Residual times relative to velocity field and Moho depth perturbations were calculated in previous studies (Grad *et al*. 2003, 2006; Starostenko *et al*. 2013a,b, 2015). It is clearly visible from the above mentioned tests that the model resolution concerning a velocity field is better than ±0.2 km s^{-1} and concerning a Moho depth is better than ±2 km within residual times of ±0.25 s. In this case, it means that more than 62 per cent of the model is determined with such an accuracy, mostly in the areas of medium and the best ray coverage (Fig. 5). The model accuracy is lower in the areas with the lowest ray coverage marked by pink colour. These areas coincide with the lowest ray paths density (Fig. 1b) caused by geometry set-up. Taking into account, that the maximal travel time error was assumed of 0.25 s for Pcr and PmP phases, this suggests that the obtained model can reproduce the travel time arrivals relatively well.

Undulating shape of the residual points in Fig. 6 is connected probably with the geometrically irregular distribution of the recordings, which has unwanted influence on the inversion code. The irregular density of seismic sources and receivers, a relatively complicated tectonic structure as well as poor 3-D geometry set-up caused higher χ^2 value and lower hit rate than desired, especially for Moho reflections and Pn phases, where the lowest data density occurs.

4 DISCUSSION

Regardless of evident imprecisions, the model gives general overview of the crustal velocity structure in the large, tectonically significant region. The model can be compiled with gravity and geomagnetic anomaly maps (Fig. 7). There are many evidenced additional pieces of model information in the areas outside the 2-D profiles. The main examples are the slices $y = 180$ from 250 to 350 km (crustal velocities of 5.5–6.5 km s^{-1}), $y = 140$ from 150 to 230 km (continent–ocean transition with sedimentary basin is characterized by very low velocities, less than 2 km s^{-1}, the Moho depth varies from 10 to 18 km, and the upper mantle velocities are around 7.5 km s^{-1}), and $y = 90$ from 300 to 350 km (upper crustal velocities around 5.5 km s^{-1}; Fig. 4).

The model (Fig. 4, right-hand column) shows crustal thinning to the north but it is rather hard to distinguish the transition to the oceanic crust. It could be determined north of Spitsbergen along a southern limit of the low gravity anomalies (Fig. 7a). The left column of Fig. 4 clearly shows variation of the structure of the passive margin of Svalbard. The thickness of continental crust decreases to the north from about 35 to 25 km (taking into account the ray coverage in Fig. 5, too). Such trend coincides with the magnetic anomalies (Fig. 7b) decreasing to the north. *P*-wave velocity ranges from 3 to 7.5 km s^{-1}. It is worth to note a high velocity area in the lower crust (HVLC, Fig. 4), in the area of the Moho slope in the vicinity of the mid-oceanic ridge. It could be caused by serpentinization connected with transform faults and active rifting or could be an intrusion connected with heating and magma flow in the vicinity of spreading processes. It additionally fits the gravity low belt going NNW from $x = 280$ km.

The continent–ocean transition is characterized by significant shallowing of Moho interface of about 20 km or more and the existence of quite large sedimentary basin with *P*-wave velocity even less than 2 km s^{-1}. This basin is less visible in the southern part of the margin where the mid-oceanic ridge is closer to the island. The transition zone is also characterized by clear change of

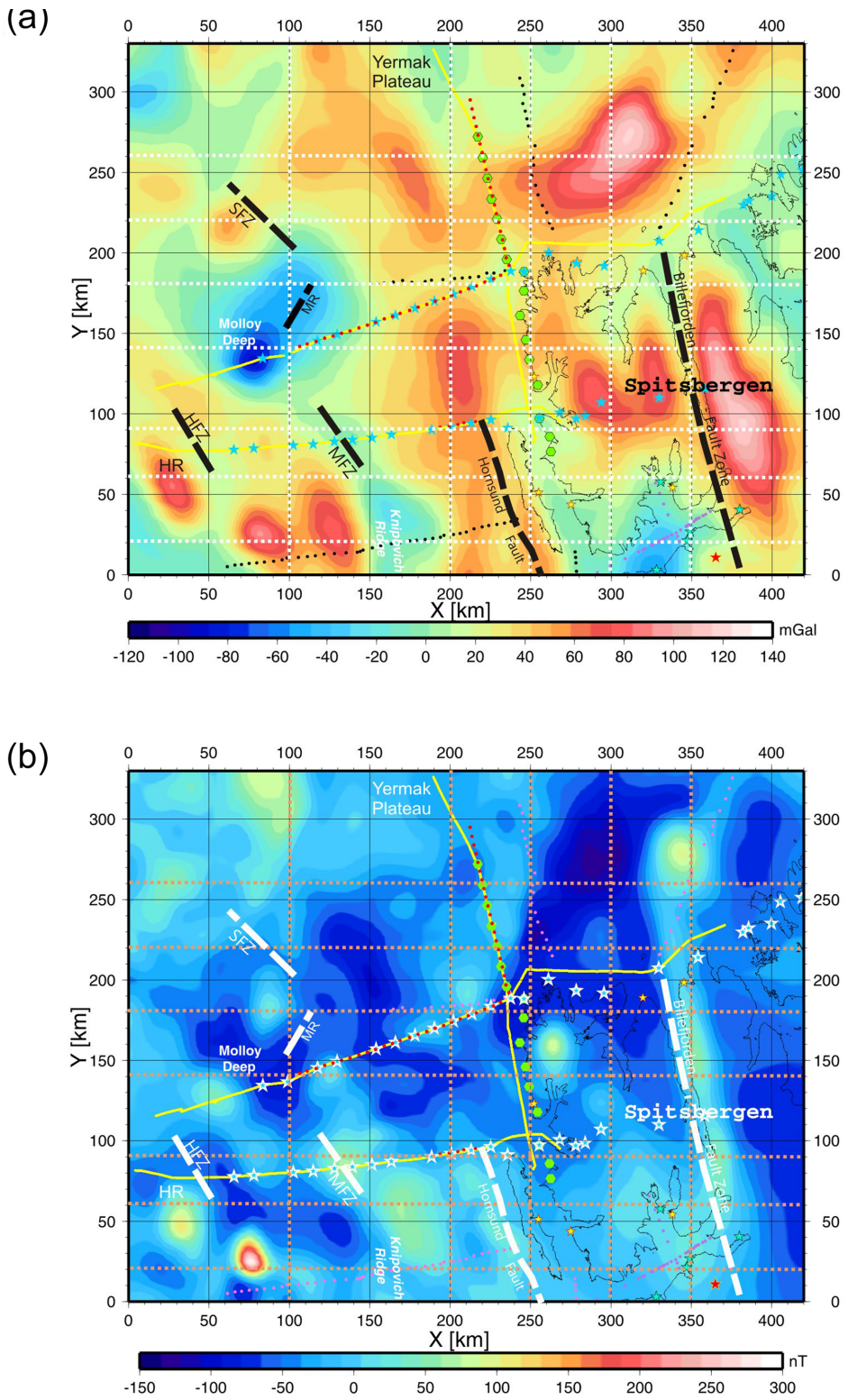

Figure 7. 3-D modelling area with (a) free air gravity anomaly map (http://earth-info.nga.mil/GandG/wgs84/agp) [Kenyon *et al*. 2008] and (b) magnetic anomaly map (http://geomag.org/models/EMAG2) [Maus *et al*. 2009] with seismic profiles and main tectonic elements. Dotted lines mark location of model slices presented in Fig. 4. Other descriptions as in Fig. 1(a).

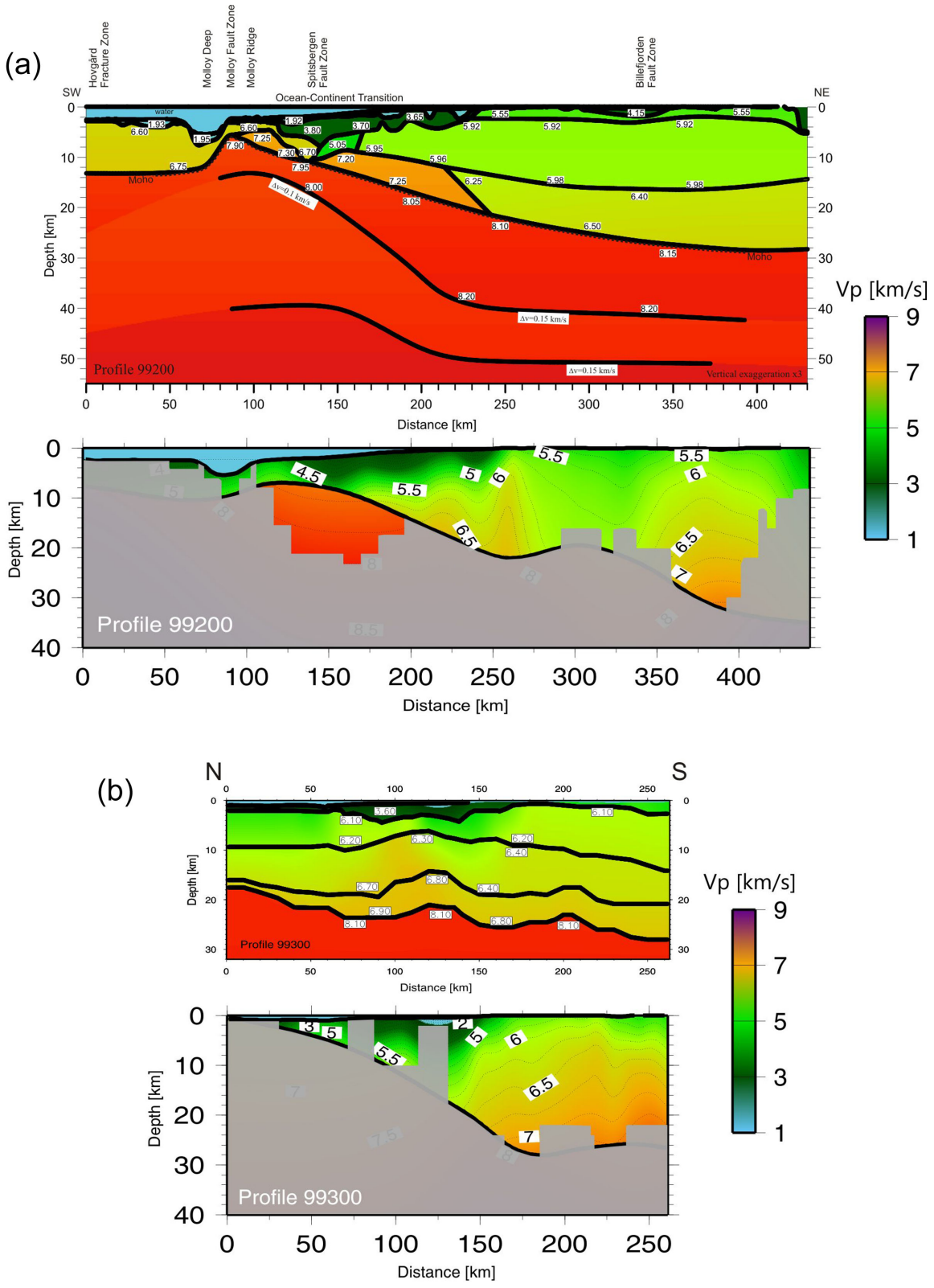

Figure 8. Comparison of the original 2-D trial-and-error models and sections of the 3-D model along the 99 200 (a) [Czuba *et al*. 2005] and 99 300 (b) [Ritzmann & Jokat 2003] profiles. Colours represent the *P*-wave velocity distribution, black thin lines – velocity isolines, black thick lines – seismic boundaries, from the 3-D model sea bottom and Moho boundary only, numbers inside white boxes – *P*-wave velocities in km s^{-1}. Grey mask marks poorly constrained parts of the 3-D model.

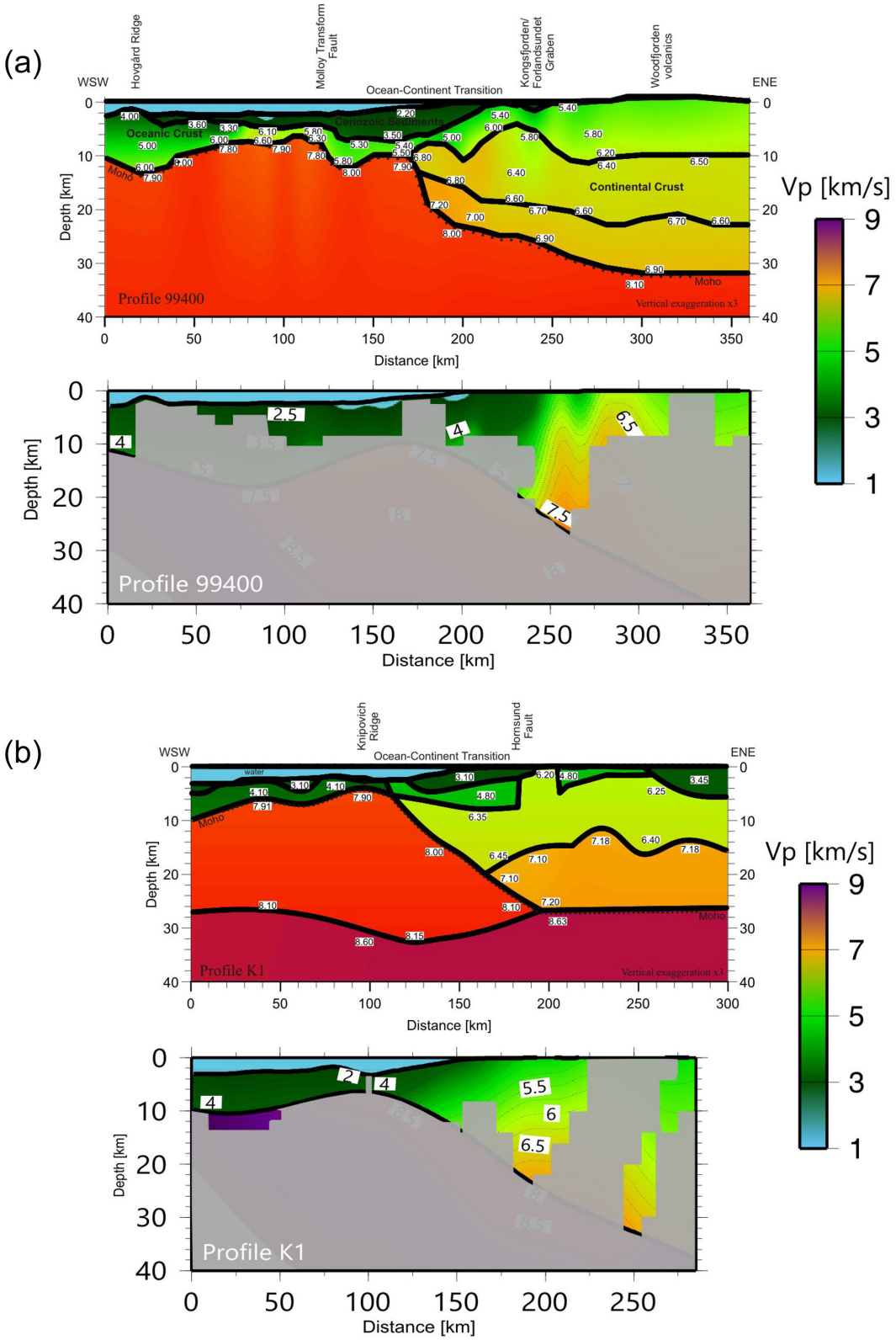

Figure 9. Comparison of the original 2-D trial-and-error models and sections of the 3-D model along the 99 400 (a) [Ritzmann *et al.* 2004] and K1 (b) [Czuba *et al.* 1999, 2004] profiles. Descriptions as in Fig. 8.

the gravity anomalies from high to low to the west. The minimal crustal thickness of about 4 km is determined in the Knipovich Ridge ($x = 170$ km, $y = 20$ km) and in the vicinity of the Molloy Deep ($x = 100$ km, $y = 140$ km), where an active rifting could occur. A low magnetic anomaly in its vicinity is observed, together with the lowest gravity anomalies. Westward, the oceanic crust is located but it is difficult to determine its exact features. In the eastern part of the study area, the Billefjorden Fault Zone is clearly marked along

gravity low and magnetic high anomaly belt. It coincides with high velocity crust at $x = 350$ km in sections $y = 180$, 220 and 260 km. Such high velocity is determined in the section $x = 350$ km at $y =$ 250–280 km what fits with local magnetic maximum.

The original 2-D model along the profile 99 200 (Fig. 8a) is generally similar except of reflectors in the mantle, which were not modelled in 3-D and the high velocity body beneath the Molloy Ridge (km 110–130), which probably was too small for the 3-D grid scale. The agreement between the models is less coincident concerning the profile 99 300 (Fig. 8b). The overall crustal velocity field is similar in the southern part of the profile, but the northern part is very sparsely sampled. This can be caused by weak PmP arrivals in this part of the profile, which were not used for the 3-D inversion. Models for profiles 99 400 (Fig. 9a) and K1 (Fig. 9b) have many similarities but there are also differences. The Moho boundary is smoother along both profiles, which is probably connected to the inversion code and size of grid cells. The Moho in the oceanic crust is interpolated deeper, which can be caused by weak PmP phases, but it fits almost exactly at the end of the profile (0–20 km) where the data are clear. The undulating shape of about 6.5 km s^{-1} isoline in the 99 400 model in the documented continental crust repeats the topography of the intracrustal boundary in the 2-D model but it is slightly moved to the right (ENE). Velocities in the sedimentary basin within the transition zone are similar.

The sections from the 3-D model, obtained using JIVE3D package, are generally similar to the 2-D models, taking into account the limits mentioned below. There are no details less than about 20 km across, such as sharp boundary or velocity changes. There is also a lack of elements evidenced by data that were not included in the 3-D modelling procedure. There are reflections from intracrustal and upper mantle boundaries which were not incorporated during picking. A number of arrivals were not used for modelling because of large uncertainty in the travel time picking. Some small elements modelled in the previous 2-D trial-and-error procedure were smoothed by the 3-D algorithm in the areas of low data density. Nevertheless, the 3-D model gives general image of the Svalbard continental margin with less unknown areas than solely 2-D profiles. The 2-D models, using more uniform data along each profile separately and using more phases, are a detailed supplement along chosen lines.

5 CONCLUSIONS

The use of in-line and off-line data recorded from several seismic experiments realized over the years allowed for 3-D tomographic seismic modelling. This is the first attempt of such crustal modelling in this region. Although the density of the data in the 3-D sense is quite low and irregular, which causes inversion problems, it is worth to have a seismic velocity model resulting from pure seismic modelling. It shows regional tectonic structure of the northwestern Svalbard region, which is characterized by passive margin features close to an active ultra-slow mid-oceanic ridge. It gives a general review of crustal structure variability of the continent–ocean transition zone along the west coast of Svalbard. The result of the seismic modelling is compared with gravity and magnetic anomaly maps. There are also information from the probable rifting area in the centre of the mid-oceanic ridge spreading axis (Figs 8a and 9b), as well as transform fault zone of the mid-oceanic ridge (Fig. 9a). The model gives also new information from areas outside the old seismic lines. The results were compared to the previous 2-D modelling, which can be treated as supplementary with more detailed information along chosen lines. Taking into account the resolution and limits of the method, there are no significant tectonic differences highlighted between the 3-D and 2-D models.

There are two places found with minimal crustal thickness of about 4 km. The uplifted Moho interface close to the Molloy Deep can be interpreted as a rift zone at the southwestern end of the Molloy Ridge possibly connected with the Molloy Transform Fault. The second place is located probably in the rift of the Knipovich Ridge.

ACKNOWLEDGEMENTS

The public domain GMT software (Wessel & Smith 1991, 1998) was used to produce most of the figures. The author is grateful to Johannes Schweitzer (NORSAR) for data recorded at the SPITS station from the 1999 experiment. This work was funded by the National Science Centre (NCN) Grant Number DEC-2012/05/B/ST10/00052. This work was partially supported within statutory activities No 3841/E-41/S/2016 of the Ministry of Science and Higher Education of Poland. The publication has been (partially) financed from the funds of the Leading National Research Centre (KNOW) received by the Centre for Polar Studies for the period 2014–2018.

REFERENCES

Birkelund, T. & Håkansson, E., 1983. The Cretaceous of North Greenland—a stratigraphic and biogeographical analysis, *Zitteliana,* **10,** 7–25.

Birkenmajer, K., 1993. Tertiary and cretaceous faulting in a proterozoic metamorphic terrain, SE Wedel Jarlsberg Land, Spitsbergen, *Bull. Polish Acad. Sci., Earth Sci.,* **41**(3), 181–189.

Breivik, A.J., Verhoef, J. & Faleide, J.I., 1999. Effect of thermal contrasts on gravity modeling at passive margins: results from the western Barents Sea, *J. geophys. Res.,* **104,** 15 293–15 311.

Burov, J.P., Krasilchikov, A.A., Firsov, L.V. & Klubov, B.A., 1977. The age of Spitsbergen dolerites, *Norsk Polarinstitutt Årbok,* **1975,** 101–108.

Crane, K., Sundvor, E., Buck, R. & Martinez, F., 1991. Rifting in the northern Norwegian-Greenland Sea: thermal tests of asymmetric spreading, *J. geophys. Res.,* **96,** 14 529–14 550.

Czuba, W., Grad, M. & Guterch, A., 1999. Crustal structure of north-western Spitsbergen from DSS measurements, *Polish Polar Res.,* **20**(2), 131–148.

Czuba, W., Ritzmann, O., Nishimura, Y., Grad, M., Mjelde, R., Guterch, A. & Jokat, W., 2004. Struktura skorupy ziemskiej w strefie krawędzi północno-zachodniego Svalbardu na podstawie badań sejsmicznych, (in Polish with English summary), in *Proceedings of the Polish Polar Studies, XXX Międzynarodowe Sympozjum Polarne*, Gdynia 2004 September 23–25, pp. 47–60.

Czuba, W., Ritzmann, O., Nishimura, Y., Grad, M., Mjelde, R., Guterch, A. & Jokat, W., 2005. Crustal structure of northern Spitsbergen along the deep seismic transect between the Molloy Deep and Nordaustlandet, *Geophys. J. Int.,* **161,** 347–364.

Czuba, W., 2013. Seismic view on the Svalbard Passive continental margin, *Acta Geophys.,* **61**(5), 1088–1100.

Dallmann, W.K., 1999. Lithostratigraphic Lexicon of Svalbard. Review and recommendations for nomenclature use. Upper Palaeozoic to Quarternary Bedrock. Review and recommendations for nomenclature use, pp. 320, Committee on the Stratigraphy of Svalbard, Norsk Polarinstitutt, Tromsø.

Davydova, N.I., Pavlenkova, N.I., Tulina, YU.V. & Zverev, S.M., 1985. Crustal structure of the Barents Sea from seismic data, *Tectonophysics,* **114,** 213–231.

Eldholm, O., Faleide, J.I. & Myhre, A.M., 1987. Continental-ocean transition at the western Barents Sea/Svalbard continental margin, *Geology,* **15,** 1118–1122.

Faleide, J.I., Myhre, A.M. & Eldholm, O., 1988. Early Tertiary volcanism at the western Barents Sea margin, *Geol. Soc. Lond. Spec. Publ.,* **39,** 135–146.

Faleide, J.I., Gudlaugsson, S.T., Eldholm, O., Myhre, A.M. & Jackson, H.R., 1991. Deep seismic transects across the sheared western Barents Sea—Svalbard continental margin, *Tectonophysics,* **189,** 73–89.

Faleide, J.I., Tsikalas, F., Breivik, A.J., Mjelde, R., Ritzmann, O., Engen, Ø., Wilson, J. & Eldholm, O., 2008. Structure and evolution of the continental margin off Norway and the Barents Sea, *Episodes,* **31**(1), 82–91.

Feden, R.H., Vogt, P.R. & Fleming, H.S., 1979. Magnetic and bathymetric evidence for the "Yermak hot spot" northwest of Svalbard in the Arctic Basin, *Earth planet Sci Lett,* **44,** 18–38.

Gabrielsen, R.H., Færseth, R.B., Jensen, L.N., Kalheim, J.E. & Riis, F., 1990. Structural elements of the Norwegian continental shelf, Part I: The Barents Sea Region, *NPD-Bulletin*, *Oljedirektoratet,* **6,** 1–33.

Grad, M. *et al.*, 2003. Crustal structure of the Trans-European suture zone region along POLONAISE'97 seismic profile P4, *J. geophys. Res.,* **108** (B11), 2541, doi:10.1029/2003JB002426.

Grad, M. *et al.*, 2006. Lithospheric structure beneath trans-Carpathian transect from Precambrian platform to Pannonian basin: CELEBRATION 2000 seismic profile CEL05, *J. geophys. Res.,* **111,** B03301, doi:10.1029/2005JB003647.

Guterch, A., Pajchel, J., Perchuć, E., Kowalski, J., Duda, S., Komber, J., Bojdys, G. & Sellevoll, M.A., 1978. Seismic reconnaissance measurement on the crustal structure in the Spitsbergen region 1976, in *Proceedings of the Geophysical Research on Svalbard,* Bergen, 61 pp.

Håkansson, E., Heinberg, C. & Stemmerik, L., 1991. Mesozoic and Cenozoic history of the Wandel Sea Basin area, North Greenland, in *Sedimentary Basins of North Greenland*, pp. 153–164, eds Peel, J.S. & Sønderholm, M., Grønlands Geologiske Undersøgelse Bulletin, 160.

Harland, W.B., 1997. The geology of Svalbard, *Geological Society Memoir,* **17**, pp. 521, The Geological Society, London.

Hobro, J.W.D., 1999. Three-dimensional tomographic inversion of combined reflection and refraction seismic travel-time data*, PhD thesis*, Cambridge: Churchill College.

Hobro, J.W.D., Singh, S.C. & Minshull, T.A., 2003. Three-dimensional tomographic inversion of combined reflection and refraction seismic traveltime data, *Geophys. J. Int.,* **152**(1), 79–93.

Hole, J.A., 1992. Nonlinear high resolution three-dimensional seismic travel time tomography, *J. geophys. Res.,* **97,** 6553–6562.

Jackson, H.R., Faleide, J.I. & Eldholm, O., 1990. Crustal structure of the sheared southwestern Barents Sea Continental margin, *Mar. Geol.,* **93,** 119–146.

Jakobsson, M., Cherkis, N.Z., Woodward, J., Macnab, R. & Coakley, B., 2000. New grid of Arctic bathymetry aids scientists and mapmakers, *EOS Trans., Am. geophys. Un.,* **81**(9), 89, **93,** 96.

Jokat, W. *et al.*, 2000. Marine Geophysics, in *The Expedition ARKTIS-XV/2 of "Polarstern" in 1999*, pp. 8–26, ed. Jokat, W., Berichte zur Polarforschung, 368, Alfred Wegener Institute for Polar and Marine Research, Bremerhaven.

Kenyon, S., Forsberg, R. & Coakley, B., 2008. New Gravity field for the Arctic, *EOS, Trans. Am. geophys. Un.,* **89**(32), 289.

Ljones, F., Kuwano, A., Mjelde, R., Breivik, A., Shimamura, H., Murai, Y. & Nishimura, Y., 2004. Crustal transect from the North Atlantic Knipovich Ridge to the Svalbard Margin west of Hornsund, *Tectonophysics,* **378,** 17–41.

Lundin, E. & Doré, A.G., 2002. Mid-Cenozoic post break-up deformation in the "passive" margins bordering the Norwegian-Greenland Sea, *Mar. Petrol. Geol.,* **19,** 79–93.

Lyberis, N. & Manby, G., 1993a. The origin of the West Spitsbergen Fold Belt from geological constraints and plate kinematics: implications for the Arctic, *Tectonophysics,* **224,** 371–391.

Lyberis, N. & Manby, G., 1993b. The West Spitsbergen Fold Belt: the result of Late Cretaceous-Palaeocene Greenland-Svalbard Convergence?, *Geol. J.,* **28,** 125–136.

Maus, S. *et al.*, 2009. EMAG2: A 2-arc-minute resolution Earth Magnetic Anomaly Grid compiled from satellite, airborne and marine magnetic measurements, *Geochem. Geophys. Geosyst.,* **10,** Q08005.

Mjelde, R. *et al.*, 2002. Geological development of the Sørvestsnaget Basin, SW Barents Sea, from ocean bottom seismic, surface seismic and potential field data, *Norw. J. Geol.,* **82,** 183–202.

Mosar, J., Eide, E.A., Osmundsen, P.T., Sommarunga, A. & Torsvik, T.H., 2002. Greenland-Norway separation: a geodynamic model for the North Atlantic, *Norw. J. Geol.,* **82**(4), 282–299.

Ohta, Y., 1994. Caledonian and Precambrian history in Svalbard: a review, and an implication of escape tectonics, *Tectonophysics,* **231,** 183–194.

Ritzmann, O. & Jokat, W., 2003. Crustal structure of northwestern Svalbard and the adjacent Yermak Plateau: evidence for Oligocene detachment tectonics and non-volcanic breakup, *Geophys. J. Int.,* **152,** 139–159.

Ritzmann, O., Jokat, W., Czuba, W., Guterch, A., Mjelde, R. & Nishimura, Y., 2004. A deep seismic transect from Hovgård Ridge to northwestern Svalbard across the continental-ocean transition: a sheared margin study, *Geophys. J. Int.,* **157**(2), 683–702.

Sellevoll, M.A., Duda, S.J., Guterch, A., Pajchel, J., Perchuć, E. & Thyssen, F., 1991. Crustal structure in the Svalbard region from seismic measurements, *Tectonophysics,* **189,** 55–71.

Starostenko, V. *et al.*, 2013a. Seismic velocity model of the crust and upper mantle along profile PANCAKE across the Carpathians between the Pannonian Basin and the East European Craton, *Tectonophysics,* **608,** 1049–1072.

Starostenko, V. *et al.*, 2013b. Mesozoic(?) lithosphere-scale buckling of the East European Craton in southern Ukraine: DOBRE-4 deep seismic profile, *Geophys. J. Int.,* **195**(2), 740–766.

Starostenko, V. *et al.*, 2015. Seismic model of the crust and upper mantle in the Scythian Platform: the DOBRE-5 profile across the Northwestern Black Sea and the Crimean Peninsula, *Geophys. J. Int.,* **201**(1), 406–428.

Steel, R.J. & Worsley, D., 1984. Svalbard's post-Caledonian strata–an atlas of sedimentational patterns and palaeogeographical evolution, in *Petroleum Geology of North European Margins*, pp. 109–135, ed. Spencer, A.M., Nor. Pet. Soc.

Sundvor, E. & Eldholm, O., 1979. The western and northern margin off Svalbard, *Tectonophysics,* **59,** 239–250.

Sundvor, E. & Eldholm, O., 1980. The continental margin of the Norwegian-Greenland Sea: recent and outstanding problems, *Trans. R. Soc. Lond., Ser. A*, **294,** 77–82.

Talwani, M. & Eldholm, O., 1977. The evolution of the Norwegian-Greenland Sea: recent results and outstanding problems, *Geol. Soc. Am. Bull.,* **88,** 969–999.

Torsvik, T.H., Løvlie, R. & Sturt, B.A., 1985. Paleomagnetic argument for a stationary Spitsbergen relative to the British Isles (Western Europe) since late Devonian and its bearing on North Atlantic reconstruction, *Earth planet. Sci. Lett.,* **75,** 278–288.

Wessel, P. & Smith, W.H.F., 1991. Free software helps map and display data, *EOS, Trans. Am. geophys. Un.,* **72,** 441.

Wessel, P. & Smith, W.H.F., 1998. New, improved version of the Generic Mapping Tools released, *EOS, Trans. Am. geophys. Un.,* **79,** 579.